

# Pneumatic Actuated Robotic Assistant System for Aortic Valve Replacement Under MRI Guidance

Ming Li\*, *Member, IEEE*, Ankur Kapoor, *Member, IEEE*, Dumitru Mazilu, *Member, IEEE*, and Keith A. Horvath

**Abstract**—We present a pneumatic actuated robotic assistant system for transapical aortic valve replacement under MRI guidance in a beating heart. This is a minimally invasive procedure that is currently performed manually inside the MRI bore. A robotic assistance system that integrates an interactive real-time MRI system, a robotic arm with a newly developed robotic valve delivery module, as well as user interfaces for the physician to plan the procedure and manipulate the robot, would be advantageous for the procedure. An Innomotion arm with hands-on cooperative interface was used as a device holder. A compact MRI compatible robotic delivery module was developed for delivering both balloon-expandable and self-expanding prostheses. A compact fiducial that can be placed close to the volume of interest and requires a single image plane was used for image-based robot registration. The system provides different user interfaces at various stages of the procedure. We present the development and evaluation of the components and the system in *ex-vivo* experiments.

**Index Terms**—MRI robot, real-time MRI (rtMRI)-guided intervention, transapical aortic valve replacement.

## I. INTRODUCTION

ONE of the minimally invasive approaches for aortic valve replacement is to implant the prosthesis through the apex of the heart. This transapical procedure is performed on the beating heart without requiring ventricular unloading. Real-time magnetic resonance imaging (rtMRI) is considered as an ideal imaging modality for this procedure due to its ability to continuously evaluate the delivery of the prosthesis and provide excellent views of valvular and annular anatomy.

Precise placement of the prosthesis in a beating heart inside an MRI scanner is a complicated task due to the limited space and awkward accessing angle. Moreover, the physician has to simultaneously manipulate multiple tools to deliver the prosthesis. Our goal is to develop a robotic system to assist in performing this minimally invasive cardiac procedure under rtMRI guidance. The robot assistance can potentially reduce the cognitive load on the physician with improved accuracy and repeatability.

Robotics has been used in cardiac surgery in an attempt to minimize the morbidity of the surgical procedures. The da Vinci

surgical robotic system has been successfully used in coronary artery bypass grafting [1], transmyocardial revascularization [2], aortic valve replacement [3], and mitral valve repair [4]. However, the present da Vinci system is not MRI compatible. MRI compatible robotic systems have been researched and developed for prostate biopsy and brachytherapy [5]–[8], breast intervention [9], [10], interventional spinal procedure [11], [12], neurosurgery [13], [14], and interventional liver therapy [15], [16]. The presence of a strong magnetic field and limited space inside an MRI scanner makes MRI compatible robot development very challenging. Contemporary researchers on medical MRI robot have primarily focused on percutaneous biopsy, drug injection, or radiotherapy seed implantation. Improving precision and accuracy, while maintaining compatibility and safety with MRI, are the prime concerns for these robotic systems.

Our group is currently focusing on developing robotic assistance for aortic valve replacement under MRI guidance [17], [18]. We reported the first generation of the system for implanting balloon-expandable (BE) prosthesis. In this paper, we detail the development and evaluation of the entire pneumatically actuated robotic assistant system for rtMRI-guided transapical aortic valve replacement. The contribution of this paper is an integrated surgical system to address the needs of the multiphases, complicated cardiac procedure. This system provides cooperative assistance to a physician, while allowing the physician to retain full control of the procedure. We present a redesigned robotic module for deploying both self-expanding (SE) and BE prostheses, and a registration method to correlate the patient heart, robot, and MRI scanner. We use a compact fiducial that can be placed close to the volume of interest (VOI) and requires a single image plane for image registration. While the structure of the marker is similar to [19], the image processing and transformation recovery methods presented in this paper are more suited for MRI inside the heart. In our system, in addition to image-guided method for robot control, we implemented interactive control, which provides direct manipulation assistance. This allows the physician to be directly in the loop to adapt the operative procedure to account for unstructured nature of our task.

## II. CLINICAL BACKGROUND

The transapical approach provides a direct and short access to the aortic annulus and enhances the ability to implant a conventional prosthesis that has known durability and proven success rate. Because the aortic valve lies in close proximity to the mitral valve and the coronary ostia, the position and orientation of the implanted prosthesis is critical. Misalignment of the prosthesis could result in mitral valve damage or cardiac ischemia.

Manuscript received May 24 2010; revised August 17, 2010; accepted October 16, 2010. Date of publication October 28, 2010; date of current version January 21, 2011. This work was supported through the Intramural Research Program of the National Heart Lung and Blood Institute and Clinical Center, National Institutes of Health, Department of Health and Human Services, USA. Asterisk indicates corresponding author.

\*M. Li is with the National Institutes of Health, Bethesda, MD 20892 USA (e-mail: lim2@mail.nih.gov).

A. Kapoor, D. Mazilu, and K. A. Horvath are with the National Institutes of Health, Bethesda, MD 20892 USA (e-mail: kapooran@mail.nih.gov; mazilud@mail.nih.gov; horvathka@mail.nih.gov).

Digital Object Identifier 10.1109/TBME.2010.2089983

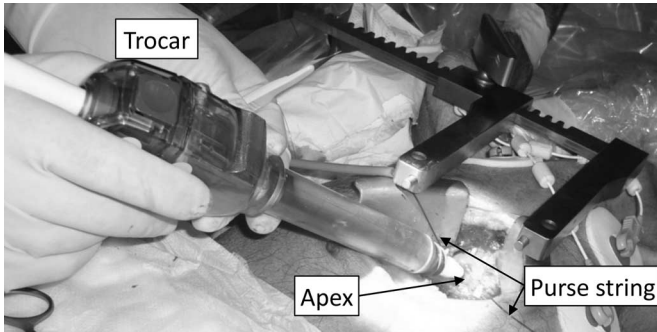


Fig. 1. Placement of a trocar during the preparatory procedure.

Typically, the distance between the aortic annulus and coronary ostia is about 9 mm, the left and right coronary artery ostia are  $120^\circ$  apart in the transaxial view. The prosthesis we used is a cylindrical shape with three commissures evenly spread at its circular base [17]. The heights of the commissure and the lowest portion between commissures are about 20 and 7 mm, respectively. To deploy the prosthesis at the optimal position, the lowest portions should be aligned with coronary ostia and the base should be placed close to the aortic annulus. Clinically, the tolerance for alignment is 3–4 mm and  $5^\circ$ .

Use of rtMRI for guidance allows physicians to monitor the progress of the procedure and also provides the ability to assess results immediately after intervention. Our group has performed the first set of rtMRI-guided transapical aortic valve replacements in an animal study [20], [21]. The trocar is first inserted into the left ventricle. Through a 6-cm chest incision, the pericardium is opened and the apex of the heart is exposed. Two concentric purse strings are placed around the apex, through which a 10–12 mm trocar is inserted into the left ventricle [20]. The physician then inserts and manipulates a long delivery device through the trocar to implant the prosthesis under rtMRI guidance. There are several obstacles to the current manual procedure. Access to the operative field inside the magnet is difficult for the physician. During the procedure, a surgical assistant holds a delivery device, on which the physician manipulates. The physician must manipulate the different components of the delivery device and other tools, such as balloon catheter or retracting wire, through the delivery device while visualizing the in-room MRI display simultaneously. In order to properly operate the interventional devices, a coordinated effort between the physician and the team is critical in the noisy MRI environment. The use of robotic assistance can alleviate the need of this level coordination between the physician and the team, provide dexterous manipulation of the interventional tools inside MRI scanner, make easy for the physician to monitor, and control the procedure effectively using the in-room display and robot control interface.

The trocar that is inserted into the apex above the diaphragm essentially anchors the heart in place (see Fig. 1). Because of the mechanical constraints, the relative motion between the aortic annulus and the apex is limited, and mainly along the long axis. As a result, robotic assistance without a sophisticated tracking mechanism is applicable to the transapical valve replacement.

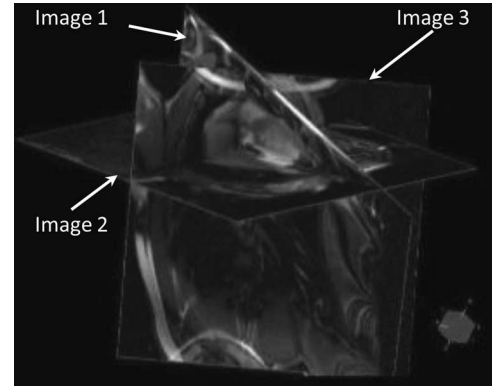


Fig. 2. Snapshot of rtMRI shows multiple image planes displayed at their relative 3-D positions. The rendering can be rotated on the in-room display to match the orientation of patient.

This situation is unique from other beating heart procedures such as mitral valve repair or coronary artery bypass.

In a minimally invasive valve replacement, either a BE or a SE stent is used to support the bioprosthetic valve and anchor it to the vessel. The procedures using these two types of prosthesis are slightly different. In a procedure with the BE prosthesis, the distal end of the loaded delivery device is first placed below the aortic annulus level, and the crimped prosthesis is then advanced to the desired position. The inflation of the balloon implant the prosthesis. In a procedure with the SE prosthesis, the loaded delivery device is first advanced into the ascending aorta, and the edge of the inner rod is placed at the aorta annulus level. The retraction of the sheath makes the crimped prosthesis expand and affix to the desired position.

### III. ROBOTIC ASSISTANT SYSTEM

The robotic assistant system for aortic valve replacement comprises three major subsystems: the imaging system, the robotic system, and user interfaces. In this section, we briefly describe each of these subsystems.

#### A. Imaging System

The imaging system provides MR sequences for surgical planning and system registration, as well as rtMRI for intervention. The rtMRI interactive system [22] consists of an interactive user interface, and operating room large screen display, specialized pulse sequences, and customized image reconstruction software. With this system, multiple oblique planes can be imaged and displayed simultaneously at their respective 3-D locations. High-quality images can be obtained at 5 frames per second. Fig. 2 shows the 3-D rendering with three image planes viewing. Image slices can be repositioned and added or omitted as needed. The MRI tissue contrast can be interactively channeled by toggling saturation pulses off/on to highlight selected objects.

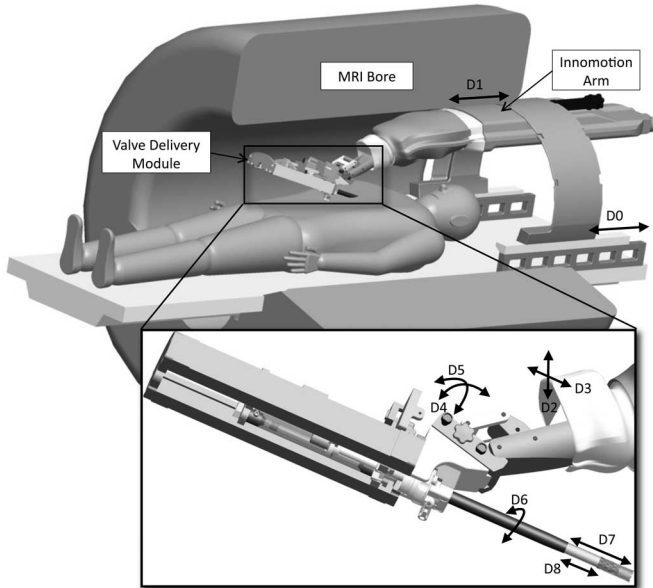


Fig. 3. CAD sketch of the robotic system with patient inside an MRI bore.

TABLE I  
ROBOT SYSTEM CHARACTERISTIC

Description of DOF	Range	Manipulation Method	Function	
D0: Gross Axial Position	300mm	Passive	Adjust robot on MR table	Positioning module
D1: Axial Translation	100mm	Hands-On, Point-to-Point	Coarse position DD	
D2: Vertical Translation	100mm			
D3: Horizontal Translation	100mm			
D4: Pitch	10-30deg	Hands-On, GUI, Point-to-Point	▷ Coarse rotate DD	VDM
D5: Yaw	±45deg		▷ Fine tune DD trajectory	
D6: Roll	±60deg	GUI, Point-to-Point	▷ Orient prosthesis	
D7: DD Translation	90mm		▷ Fine position prosthesis	
D8: DD Insertion	45mm		▷ Deploy prosthesis	

DD = delivery device.

### B. Robotic System

The CAD sketch of the robotic system, which operates in the confined space between the MRI bore and the supine patient is shown in Fig. 3. The descriptions and functions of all 9 degree of freedom (DOF) are listed in the Table I. Different manipulation methods, namely, point-to-point, hands-on, and interactive graphic user interface (GUI) were implemented for communication between the robot system and the interface system.

The robotic system comprises two components: a 5-DOF positioning module and a 3-DOF (VDM). The robotic VDM was designed for manipulating and placing the prosthesis inside MRI scanner. The detail of this module is presented in Section IV. An MRI compatible Innomotion arm [11] (Innomedic, Herxheim, Germany) was employed to hold the robotic module and move the valve delivery device on its planned trajectory. The robotic

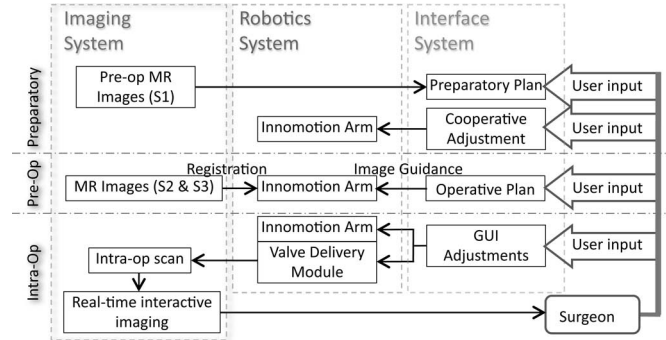


Fig. 4. Diagram showing connections between different subsystems and interactions of the physician with the system.

arm has a remote center of motion (RCM) structure and its configuration fits into a standard closed MRI scanner.

### C. User Interfaces and Workflow

Transapical aortic valve replacement has three distinct phases, namely, preparatory, preoperative, and intraoperative. We implemented different interfaces—cooperative adjustment, operative plan, and interactive GUI adjustments—to suit the needs at the different phases. The interactions between the subsystems and the physician are shown in Fig. 4.

First the patient undergoes an MRI scan (S1) for the physician to determine the aortic annular diameter, coronary ostial anatomy, and apical location. In the preparatory phase, after the patient is intubated and anesthetized, the physician places the trocar into the heart. The Innomotion robotic arm is then mounted on the MRI table and adjusted such that its end effector is close to the trocar port. The robotic VDM with a fiducial rod attached is mounted on the Innomotion arm. The physician uses cooperative hands-on interface [23] to adjust the Innomotion arm to insert the fiducial rod into the trocar. Once the fiducial rod is in place, the user input sensor is detached and the robot is moved into the bore.

In the preoperative phase, the patient undergoes another MRI scan (S2) for the physician to plan the trajectory of the delivery device. At the same time, another MR sequence (S3) is used for system registration. The Innomotion arm is moved to the planned trajectory, under image guidance using images from scan S2. The MRI table is then moved out, and the fiducial rod is replaced by the delivery device. Thus, direct access to the aortic annulus is created.

In the intraoperative phase, the physician uses the visual feedback from the rtMR imaging, and interactively adjust and deploy the prosthesis using the VDM via a GUI.

## IV. ROBOTIC VALVE DELIVERY MODULE

The robotic module is presumed to be placed inside the MRI scanner close to the isocenter and operated during imaging. The presence of a strong magnetic field inside the MRI scanner demands that the robotic module must be MRI compatible [24], [25]. To maintain image quality and prevent local heating in the

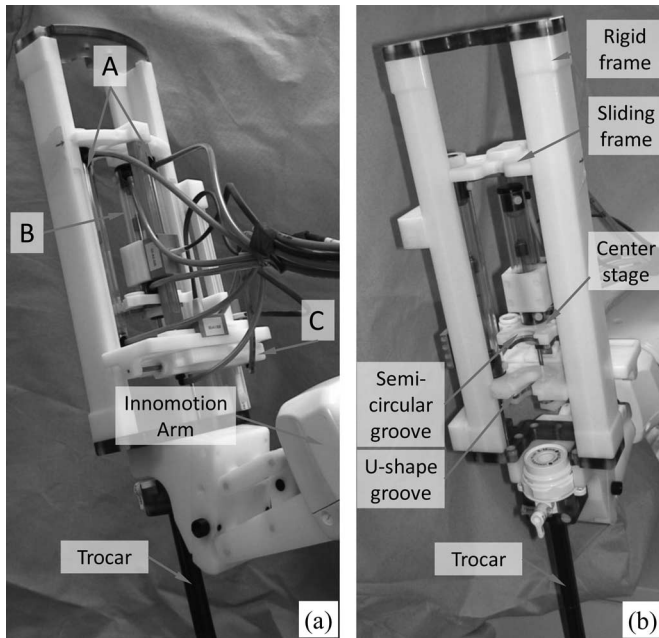


Fig. 5. Prototype of robotic VDM, (a) back view and (b) front view.

proximity of the patient, nonconductive plastic materials, such as Delrin, Ultem, and Polyetheretherketones (PEEK) were used.

The robotic module is designed for manipulating a delivery device to position and deploy the prosthesis. The delivery device consists of a 30-cm-long straight plastic inner rod. A hollow outer sheath protects the loaded prosthesis before it is deployed.

#### A. Mechanical Design and Implementation

The robotic module comprises two linear joints: the translation joint “A” and the insertion joint “B,” as well as a rotational joint “C” (see Fig. 5). The operations of the linear joints and the rotational joint are independent. Two linear joints can be independently or simultaneously controlled.

The translation joint (D7) provides linear displacement of the delivery device (both its inner rod and protecting sheath) along its axis. This joint is directly actuated by two parallel linear pneumatic actuators. The two-actuator structure guarantees balanced motion of a delivery device. The bodies of two linear actuators, together with a base plate and a top plate form a sliding frame. The sliding frame can slide on two frame rails. These two frame rails, together with a connecting plate and a top plate form a rigid frame. The connecting plate has grooves that match a corresponding adaptor on the last joint of the Innomotion robotic arm.

The rotational joint (D6) rotates the delivery device around its axis. This changes the orientation of the loaded prosthesis. It is actuated by a linear pneumatic actuator attached on the base plate of the sliding frame. The linear movement is transmitted to the rotational movement by a rack-gear transmission.

The insertion joint (D8) moves only the inner rod of the delivery device, thus advancing the loaded prosthesis out of the protecting sheath. It is actuated by a linear pneumatic actuator

mounted on a central stage. This central stage can move back and forth inside the sliding frame.

A semicircular groove embedded on the central stage holds the inner rod of the delivery device. A U-shape groove installed on the base rack of the sliding frame holds the sheath of the delivery device. The semiopen structure of grooves is designed for easy attachment of the sterilizable delivery device.

The VDM supports deploying both the BE and the SE prosthesis. Sole motion of the insertion joint moves only the inner rod of the delivery device, driving the BE prosthesis out of the protecting sheath to the desired position. Simultaneously retracting the translation joint and advancing the insertion joint at the same velocity keeps the inner rod of the delivery device at its location, and retracts the protecting sheath back to expose the prosthesis. This simultaneous motion will let the crimped SE prosthesis expand and affix to the desired position.

#### B. Actuators, Sensors, and Control

Pneumatic actuators were used in the robotic module. These compact MRI compatible pneumatic actuators are made of glass cylinders, graphite pistons, brass shafts, and plastic housings (Airpel, Norwalk, CT, USA). Two DS15GV pneumatic pressure servovalves (GAS Automation GmbH, Germany) were used to maintain and modulate the air flow between two outputs corresponding to two chambers of one cylinder. These pneumatic valves were located outside the 5-G line. A set of 5-m long air hoses were used for the pneumatic connections between the servovalves and the robotic module.

Magnetotranslucent fiber-optical incremental encoders (Innomedic, Herxheim, Germany) made of glass were used to gather positioning information. The optical resolution is 0.002 mm. Optical fibers transferred the signals to optoelectronic conversion circuits located outside the 5-G line.

A 2-GHz Pentium IV computer running Windows XP operating system with an XMP-SynqNet-PCI hardware interface (Motion Engineering Inc, St Barbara, CA, USA) was used for module control. A PIV (proportional position loop integral and proportional velocity) controller running on the DSP-based board is used for servoing the position. The control PC was placed outside of the MR room. It communicated with the electronic devices that control pneumatic valves and read encoder signals via the optic network.

To provide accurate position control, we targeted the accuracy of the linear joints to be around 1 mm and the accuracy of the rotation joint as  $1^\circ$ . In addition to this point-to-point position move mode, we implemented a continuous control mode (velocity mode) to provide an interactive control interface. With the continuous mode, the physician can start, stop, or resume the joint motion any time he/she decides, therefore, he/she can monitor and control the progress during the prosthesis deployment. In the point-to-point mode, the accuracy of the target position is the priority. The continuous mode demands a smooth motion without oscillations during the transmission, i.e., the velocity error during the transmission should be small. It requires the compromise between the smoothness, velocity, and position error.

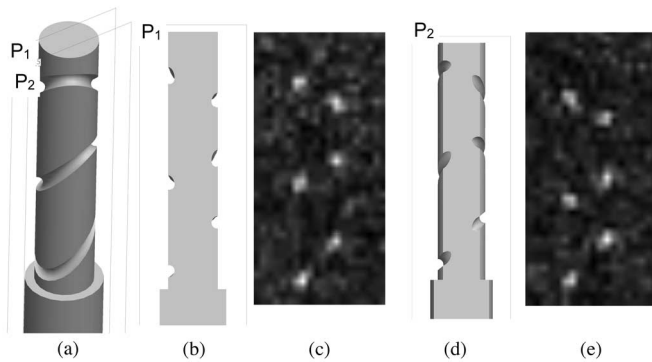


Fig. 6. (a) CAD drawing of fiducial with three elliptical patterns. (b) and (d) Cross-section of fiducial through planes P1 and P2, respectively. (c) and (e) MRI image corresponding to (b) and (d), respectively.

## V. SYSTEM REGISTRATION

Coil-based [6] and image-based registrations [26], [27] are commonly used in MRI-guided systems. Coil-based registration provides real-time data but is scanner dependent. Image-based registrations are scanner independent but are not real time. We noticed that the fiducials used for image-based registrations are placed at some distance away from the tip of the interventional tool or the VOI [26], [27]. In the valve replacement procedure, a multichannel body coil is used, and the volume that can be acquired with sufficient image quality is of limited size. Thus, a fiducial close to the VOI and image isocenter is preferred. Moreover, registration of the robot prior to the placing the patient on the table (and thus being able to place the fiducial at the isocenter) is not practical in this case, as a preparatory procedure of inserting the trocar is performed on the MRI table. In this section, we present the details of image-based registration using a compact elliptical fiducial that can be placed in the VOI.

### A. Fiducial and MRI sequences

The fiducial rod [see Fig. 6(a)] comprises three elliptical grooves filled with diluted gadolinium (0.01 mol/L). The fiducial rod is 50-mm long and 11 mm in diameter. The diameter of the groove is 2.6 mm.

The MRI sequence that we used for the registration is Siemens TrueFISP\_IR, fast imaging with steady-state precession with inverse recovery pulse using standard body coil. A good choice of parameter of inversion time will suppress both blood and myocardium signal. The parameters of the sequence we used for acquiring a bright signal of the fiducial is as follows: TR = 800 ms; TE = 2 ms; TI = 706 ms; flip angle = 50°; slice thickness = 1.05 mm; FOV = 188 × 287; and matrix = 126 × 192. The image plane is chosen to pass through or nearly pass through the center line of the fiducial such that the image plane intersects with the three ellipses to obtain six bright fiducial points, as shown in Fig. 6.

### B. Image Processing

A straightforward method to determine these image points uses intensity-weighted centroids of threshold-filtered image.

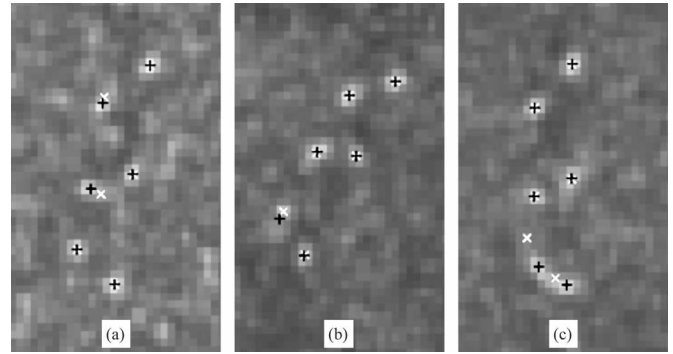


Fig. 7. Image processing results for fiducial localization. “+”: Output of least-squares fitting. “×”: Output of weighted centroid. (a) and (b) Recovering fiducial points with background noise. (c) Recovering fiducial points on the end slabs.

Due to the sizes of the fiducial image points, which are only 4–5 pixels, and the noise from the surrounding environment, localization error could be relatively large. We propose a new method to increase the accuracy of localization. We assume that each of these fiducial image points has a Gaussian intensity distribution, and use least-squares fitting to obtain the parameters of the Gaussian that match each of the six fiducial points

$$\min_{(x_i, y_i, \mathbf{P}_i)} \left\| \sum_{i=1}^6 g_i(x_i, y_i, \mathbf{P}_i) - \mathbf{I}_{\text{smooth}} \right\|^2 \quad (1)$$

where,  $\mathbf{I}_{\text{smooth}}$  is a Gaussian smoothed intensity image (kernel size = 5 × 5,  $\sigma = 0.65$ ) and  $g_i(x_i, y_i, \mathbf{P}_i)$  are the six Gaussian intensity distribution, with mode  $(x_i, y_i)$  and parameters  $\mathbf{P}_i$ . The starting point for the nonlinear least-squares problem is obtained from the intensity-weighted centroids of a threshold-filtered image.

We have observed that the least-squares fitting improves robustness especially in cases when the image points are non-circular due to partial volume effect and noises in the region of interest [see Fig. 7(a) and (b)]. The aforementioned MRI sequence provides a series of ten slabs with 1.05-mm spacing for each scan. The central slabs are close to the centerline of the fiducial, while the slabs toward two ends meet the edges of the fiducial. The image points on the central four to six slabs are circular and easily localized, while, those on the end slabs are elongated and more difficult to localize [see Fig. 7(c)]. On an average, the least-squares fitting rectifies the location by 0.33 ± 0.42 mm (max. 6.32 mm,  $n = 534$  points in 89 images).

### C. Transformation Recovery

The next step is to determine the transformation between the fiducial frame and the image frame based on these image points and the geometry of the fiducial. The origin of the fiducial frame is defined at the center of the middle ellipse;  $z$ -axis is the centerline of the fiducial;  $xy$ -plane is perpendicular to  $z$ -axis. Let  $(\mathbf{R}_{\Pi}, \mathbf{T}_{\Pi})$  be the transformation of the plane patch  $\Pi$  in the fiducial frame. We first find the plane patch  $\Pi$  that can best represent the image plane, and then use point-to-point registration to recover the transformation. The algorithm is described as follows.

- 1) We first prematch the image plane to the plane patch  $\Pi$ . We defined a local frame  $\mathbf{F}_c$  in the orthogonal coordinate system of the eigenvectors centered at the center of mass of the six image points  $\mathbf{P}_i$ . The  $z$ -axis is parallel to the eigenvector with the largest eigenvalue, and the  $x$ -axis is parallel to the eigenvector with the smallest nonzero eigenvalue,  $y$ -axis is perpendicular to  $xz$ -plane. We then transform six image points into the frame  $\mathbf{F}_c$ , and obtain  $\mathbf{P}_{c,i} = \mathbf{F}_c^{-1} \times \mathbf{P}_i$ .
- 2) Let  $\mathbf{P}_{f,i}$  be the points of the intersection of plane  $\Pi$  with the fiducial in the fiducial frame.  $\mathbf{p}_{f,i}$  are the projection of  $\mathbf{P}_{f,i}$  on the plane  $\Pi$ . We try to find the plane patch  $\Pi$  such that  $\mathbf{p}_{f,i}$  best match  $\mathbf{p}_{c,i}$ , which are the projection of  $\mathbf{P}_{c,i}$  on the image plane. We can form a constrained nonlinear optimization problem

$$\mathbf{P}_{f,i}^* = \min_{\Pi} \|\mathbf{p}_{f,i} - \mathbf{p}_{c,i}\|^2. \quad (2)$$

$\mathbf{P}_{f,i}^*$  are the points in the fiducial frame that minimize the objective. A good guess of the start point for the nonlinear optimization problem is based on the assumption that the image plane passes through the center line of the fiducial. In this case,  $(\mathbf{R}_{\Pi}, \mathbf{T}_{\Pi})$  can be simplified as  $(\mathbf{Rz}(\phi), \mathbf{0})$ , where  $\phi$  is the rotation angle around the  $z$ -axis of the fiducial frame. We rotate the plane patch  $\Pi$  around the center line  $\mathbf{Rz}(\phi)$  and determine  $\phi$  such that it minimizes  $\|\mathbf{p}_{f,i} - \mathbf{p}_{c,i}\|^2$ .

- 3) We now have corresponding point pairs,  $\mathbf{P}_{f,i}^*$  and  $\mathbf{P}_i$ , in the fiducial frame and the image frame, respectively. The transformation  ${}^f\mathbf{T}_i$  can be computed by point-to-point registration methods. The six points obtained from a single slab are sufficient to recover the transformation, however, since the MRI sequence provides a series of ten slabs, we have more information to improve the accuracy of the registration. We repeat Step 2 for all the slabs that have six identifiable, bright intensity points corresponding to the intersection of the image plane with the fiducial. Typically four to six slabs are available to obtain corresponding point pairs resulting in 24–36 pairs. Thus, the transformation  ${}^f\mathbf{T}_i$  can be solved in a least-squares sense using all these points.

## VI. EVALUATIONS

We evaluated the components of our system and the overall system. A summary of these results as well as the overall error in placement of the prosthesis is shown in Table II.

### A. Valve Delivery Module

We tested the prototype of the robotic VDM that is shown in Fig. 5. The air pressure for actuating the pneumatic pistons was 75 psi (520 kPa). The maximum force load of the translation joint was 34 N. The maximum torque of the rotation joint was 0.4 Nm.

We evaluated the accuracy of the robotic module under the point-to-point mode. With a maximum operational velocity of 10 mm/s, the accuracy of the linear joints was  $0.19 \pm 0.14$  mm.

TABLE II  
SUMMARY OF COMPONENT AND SYSTEM EVALUATIONS

Description	Test Condition	Result
<b>Valve Delivery Module*</b>		
Linear Error	Point-to-Point; at 10mm/s	$0.19 \pm 0.14$ mm
Orientation Error	Point-to-Point; at 5deg/s	$0.46 \pm 0.27$ deg
Velocity Error	Sole joint motion; Interactive GUI	<0.5mm/s
Velocity Error	Simultaneous motion;	<0.5mm/s
Position Error	Interactive GUI	<0.5mm
<b>MRI compatibility</b>		
SNR Loss	SSFP sequence; Robot in scanner & in motion	8.2%
<b>Registration Accuracy</b>		
Craniocaudal direction	Elliptical pattern fiducial with multiple image slabs	$0.62 \pm 0.50$ deg
Axial direction		$0.36 \pm 0.30$ deg
<b>Prosthesis Deployment*</b>		
Placement Error	without rtMRI guidance, i.e. with direct visualization	$0.80 \pm 0.40$ mm
	with rtMRI guidance	$1.14 \pm 0.33$ mm

\* These results were obtained under the load as experienced during manual prosthesis deployment, majority of which arises from the friction with the trocar (maximum friction force  $\approx 12$ N).

With a maximum operational velocity of  $5^\circ$  per second, the rotation joint was  $0.46^\circ \pm 0.27^\circ$ .

We also evaluated the smoothness, speed, and error of two linear joints under the continuous mode. We moved the translation and insertion joints of the robot in the continuous mode and recorded their position and velocity using the encoders (resolution  $2 \mu\text{m}$ ). In this mode, the maximum position error of the translation joint is less than 0.3 mm and its maximum velocity error is less than 0.2 mm/s. The maximum position error of the insertion joint is less than 0.5 mm and its maximum velocity error is less than 0.2 mm/s. Simultaneous motion of the linear joints, for the SE prosthesis deployment, had a maximum position error of less than 0.5 mm, and maximum velocity error was less than 0.5 mm/s.

### B. MRI Compatibility

We evaluated the MR compatibility of the entire robotic system with a 1.5T Siemens Espree scanner. A 16-cm cylindrical MR phantom was placed at the isocenter. A steady-state free precession (SSFP) sequence was used with following scanning parameter: TR = 436.4 ms; TE = 1.67 ms; echo spacing = 3.2 ms; bandwidth = 1000 Hz/pixel; flip angle =  $45^\circ$ ; slice thickness = 4.5 mm; FOV =  $340 \times 283$  mm; and matrix =  $192 \times 129$ . This protocol is similar to the one we used in MR scanning for the cardiac intervention. The imaging series were taken with: 1) phantom only, and 2) robotic system placed in the magnet and running during imaging. In the latter case, the robotic module was mounted on the Innomotion arm, its distal end was at a distance of 150 mm from the center of the image area.

The presence and motion of the robotic system inside the scanner was found to have no noticeable disturbance in the image. The observed SNR loss was 8.2% for the entire robotic system placed in the scanner and in motion. The SNR was calculated using the definition as the mean value of the 24 cm<sup>2</sup>

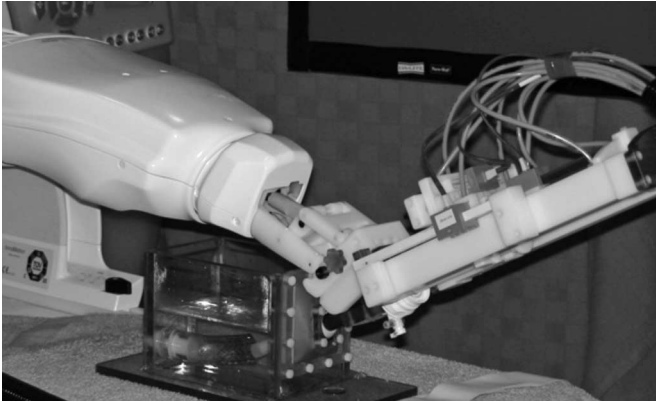


Fig. 8. Setup for system level evaluation on a phantom.

area at the center of the image divided by the standard deviation of the 24 cm<sup>2</sup> area in the lower right corner of the image.

### C. Registration Accuracy

The purpose of the registration in our application is to command the robotic arm to adjust the delivery device to the pre-planned trajectory. The path of the preplanned trajectory passes the apex, which usually is prelocated at the RCM of the Innomotion robot. Therefore, the rotation accuracy is more important in our case.

The fiducial was rigidly fixed to the Innomotion robot that was mounted on the MRI table. The fiducial was submerged under water. The robot was commanded to rotate around RCM, first to rotate and stop at seven different poses in the *craniocaudal* direction and then seven different poses in the *axial* direction of the MRI scanner. We recorded the robot joints at each pose and calculated the relative angular values between any of the two poses. These values served as the ground truth. We also scanned the fiducial at each pose and computed the rotation from the scanner coordinate frame to the fiducial coordinate frame,  ${}^s\mathbf{T}_f$ .

We calculated the Euler angles between any of two poses based on the computed  ${}^s\mathbf{T}_f$ . The rotation errors using single centermost slab in craniocaudal and axial directions are  $0.81^\circ \pm 0.74^\circ$  and  $0.19^\circ \pm 0.17^\circ$ , respectively. The rotation errors using all slabs in craniocaudal and axial directions are  $0.62^\circ \pm 0.50^\circ$  and  $0.36^\circ \pm 0.30^\circ$  deg, respectively. As a comparison, the transformation is also computed for the same set of poses using the marker provided along with the Innomotion robot [11]. This marker consists of four spherical hollow balls (overall dimensions: 100 × 80 × 20 mm) filled with MR contrast agent rigidly attached to the last joint of the Innomotion robot. The rotation errors using these large spherical markers in craniocaudal and axial directions are  $0.63^\circ \pm 0.72^\circ$  and  $0.36^\circ \pm 0.33^\circ$ , respectively. Due to its construction this marker is approximately 15 cm away from the VOI. Further, the robot registration using this marker can only be done before the patient is placed on the table.

### D. System Level Evaluation

The motivation of our phantom based experiment (see Fig. 8) is to test the feasibility of the integrated system from the en-

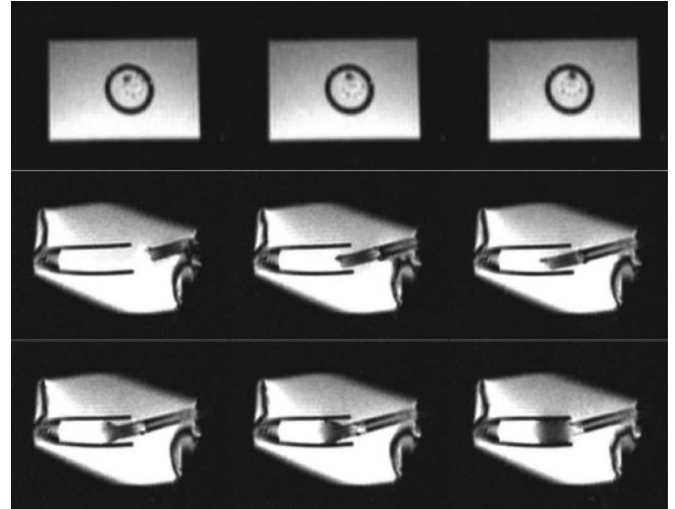


Fig. 9. Sequence of MR images showing the progress of using our robotic system to place a prosthesis under MRI guidance. First row shows the orientation adjustment of the prosthesis. Second row shows the position adjustment of the prosthesis. Third row shows the deployment of the SE prosthesis.

gineering point of view. A phantom was designed to emulate the dimensions of the valve replacement situation. It consisted of a plastic tube with 25-mm diameter, which served as the aorta. The diameter of the tube is typical size of adult human aortic root. This was mounted on one side of a 200 × 100 × 100 mm water tank. A spherical joint mounted on a flexible, elastic membrane located on the opposite side of the tank, served as the apex. A 12–15-mm trocar was inserted into the spherical joint. The distance from spherical joint to the end of the plastic tube was 50 mm, which is the typical distance from the heart apex to the aorta annulus as measured in clinical scenario. The trocar insertion point had some compliance due to the mounting arrangement.

We tested the robotic system for SE prosthesis deployment. The SE prosthesis requires coordinated motion between two coupled pneumatic joints, thus making it a more challenging scenario. We aimed to deploy the SE prosthesis such that its proximal edge is on the edge of the tube under rtMRI guidance using robotic system.

Fig. 9 shows the progress of the orientation adjustment and the position adjustment of the prosthesis, as well as the progress of the deployment of the SE prosthesis. After the prosthesis was deployed, we measured the distance between the edge of the tube and the edge of the SE prosthesis by caliper, and defined it as the position error. The average of absolute system level error over seven trials was  $1.14 \pm 0.33$  mm.

To evaluate the performance of the robotic system without the error associated with rtMRI guidance, we also performed the valve deployment experiment with direct visualization. The average distance based on nine trials for a SE prosthesis was  $0.8 \pm 0.4$  mm, representing the cumulative error from robotic arm, the VDM, and the motion and/or slippage of the prosthesis during the deployment, but not due to MRI guidance. The most likely reason for the difference can be attributed to the low spatial and temporal resolution of rtMRI.

## VII. DISCUSSION AND CONCLUSION

We developed a robotic assistant system for assisting in transapical aortic valve replacement under rtMRI guidance. Our system integrates a rtMRI system, a robotic arm with a newly developed robotic VDM, as well as user interfaces for the physician to plan the procedure and manipulate the robot. The presence and motion of the robotic system inside the MRI scanner was found to have no noticeable disturbance in the image.

A compact 3-DOF robotic VDM was designed and constructed for manipulating and placing both BE and SE prosthesis into a heart inside MRI scanner. We have shown the robotic module possesses sufficient position and velocity accuracy.

We used a compact fiducial pattern placed in the VOI for robot registration. This fiducial allows minimal disruption of the workflow during the preparatory procedure of placing the trocar and inserting the delivery device using hands-on cooperative interface. The MRI sequence used for imaging the fiducial successfully suppressed the signal from the blood and the myocardium, enabling suitable localization of gadolinium filled fiducial. With a new localization and transformation recovery method, this compact fiducial leads to registration accuracy comparable to the result by using a larger marker, which can only be placed 15 cm away from the VOI.

We proposed multiple interfaces for the valve replacement procedure. We believe, that in the engineering of robots for medical applications, detailed analyses of the functions of the entire system, i.e., robot, interfaces, and application, taken as single entity, is arguably more important than the individual performance of the subsystems (robot, physician, interfaces, and application, separately). Thus, having a combination of more than one interface such as image guided, console guided, or hands-on based on application might yield a higher performance from the entire system.

We tested the integrated system with a phantom. The results show that all subsystem cooperate smoothly to provide assistance for bioprosthetic aortic valve replacement. The stable phantom is not an ideal replica of the beating heart. But with proper anatomical dimension between the aortic annulus and the apex, it provides a reasonable situation to validate the coordinated working of the different components of the integrated system before sacrificing animal lives.

As mentioned, the mechanical constraints provided by the trocar that is inserted into the heart apex anchors the heart. Based on our experience on the manual procedure, we note that with the trocar in place, the relative motion of the aortic annulus with respect to the apex is limited and mainly along the long axis. Interactive control, which provides direct manipulation assistance allows the physician to be directly in the loop to adapt the operative procedure to account for this motion. The physician, who performs manual valve replacement evaluated the system in a phantom study and commented that the use of the system minimized the cognitive burden of manipulation of multiple tools from awkward angles, and the interactive interface kept the first hand control on the procedure. The performance of using interactive interface to control the system in a beating heart shall be further evaluated in our future work in an animal study.

## ACKNOWLEDGMENT

M. Li and A. Kapoor contributed equally to this work.

## REFERENCES

- [1] V. Falk, S. Jacobs, J. Gummert, T. Walther, and F. Mohr, "Computer-enhanced endoscopic coronary artery bypass grafting: The da Vinci experience," *Semin. Thorac. Cardiovasc. Surg.*, vol. 15, no. 2, pp. 104–111, 2003.
- [2] D. D. Yuh, B. A. Simon, A. Fernandez-Bustamante, N. Ramey, and W. A. Baumgartner, "Totally endoscopic robot-assisted transmyocardial revascularization," *J. Thorac. Cardiovasc. Surg.*, vol. 130, pp. 120–124, 2005.
- [3] T. Folliguet, F. Vanhuyse, D. Magnano, and F. Laborde, "Robotic aortic valve replacement: Case report," *Heart Surg Forum*, vol. 7, pp. E551–E553, 2004.
- [4] L. Nifong, V. Chu, B. Bailey, D. Maziarz, V. Sorrell, D. Holbert, and J. W.R. Chitwood, "Robotic mitral valve repair: Experience with the da Vinci system," *Ann Thorac Surg*, vol. 75, pp. 438–443, 2003.
- [5] K. Chinzei, N. Hata, F. Jolesz, and R. Kikinis, "MR compatible surgical assist robot: System integration preliminary feasibility study," *Med. Image Comput. Comput.-Assist. Intervention Conf. (MICCAI)* (Lecture Notes in Computer Science, vol. 1935), pp. 921–930, 2000.
- [6] A. Krieger, R. Susil, C. Menard, J. Coleman, G. Fichtinger, E. Atalar, and L. Whitcomb, "Design of a novel MRI compatible manipulator for image guided prostate interventions," *IEEE Trans. Biomed. Eng.*, vol. 52, no. 2, pp. 306–313, Feb. 2005.
- [7] G. S. Fischer, I. Iordachita, S. DiMaio, and G. Fichtinger, "Development of a robotic assistant for needle-based transperineal prostate interventions in MRI," *Med. Image Comput. Comput.-Assist. Intervention (MICCAI)*, (Lecture Notes in Computer Science, vol. 4791), pp. 425–453, 2007.
- [8] D. Stoianovici, D. Song, D. Petrisor, D. Ursu, D. Mazilu, M. Mutener, M. Schar, and A. Patriciu, "MRI Stealth" robot for prostate interventions," *Minimally Invasive Therapy All. Technol.*, vol. 16, pp. 241–248, 2007.
- [9] W. A. Kaiser, H. Fischer, J. Vagner, and M. Selig, "Robotic system for biopsy and therapy of breast lesions in a high-field whole-body magnetic resonance tomography unit," *Invest Radiol.*, vol. 35, pp. 513–519, 2000.
- [10] B. T. Larson, A. Erdman, N. Tsekos, E. Yacoub, P. Tsekos, and I. Koutlas, "Design of an MRI-compatible robotic stereotactic device for minimally invasive interventions in the breast," *J. Biomech. Eng.*, vol. 126, pp. 458–465, 2004.
- [11] E. Hempel, H. Fischer, L. Gumb, T. Hohn, H. Krause, U. Voges, H. Breitwieser, B. Gutmann, J. Durke, M. Bock, and A. Melzer, "An MRI-compatible surgical robot for precise radiological interventions," *Comput. Aided Surg.*, vol. 8, pp. 180–191, 2003.
- [12] A. Melzer, B. Guttman, T. Remmele, R. Wolf, A. Lukoscheck, M. Bock, H. Bardenheuer, and H. Fischer, "MRI and CT compatible robotic system for percutaneous image guided interventions: Principles and evaluation," *IEEE Eng. Med. Biol. Mag.*, vol. 27, no. 3, pp. 66–73, 2008.
- [13] K. Masamune, E. Kobayashi, Y. Masutani, M. Suzuki, T. Dohi, H. Iseki, and K. Takakura, "Development of an MRI-compatible needle insertion manipulator for stereotactic neurosurgery," *J. Image Guid Surg.*, vol. 1, pp. 242–248, 1995.
- [14] Y. Koseki, T. Washio, K. Chinzei, and H. Iseki, "Endoscope manipulator for trans-nasal neurosurgery, optimized for and compatible to vertical field open MRI," *Med. Image Comput. Comput.-Assist. Intervention (MICCAI)*, (Lecture Notes in Computer Science, vol. 2488), pp. 114–121, 2002.
- [15] N. Hata, T. Junichi, S. Hurwitz, and S. Morikawa, "MRI-compatible manipulator with remote-center-of-motion control," *J. Magn. Reson. Imag.*, vol. 27, pp. 1130–1138, 2008.
- [16] D. Kim, E. Kobayashi, T. Dohi, and I. Sakuma, "A new, compact MR-compatible surgical manipulator for minimally invasive liver surgery," *Med. Image Comput. Comput.-Assist. Intervention (MICCAI)*, (Lecture Notes in Computer Science, vol. 2488), pp. 164–169, 2002.
- [17] M. Li, D. Mazilu, and K. A. Horvath, "Robotic system for transapical aortic valve replacement with MRI guidance," *Med. Image Comput. Comput.-Assist. Intervention (MICCAI)*, (Lecture Notes in Computer Science, vol. 5242), pp. 476–484, 2008.
- [18] M. Li, A. Kapoor, M. Dumitru, B. Wood, and K. A. Horvath, "Cardiac interventions under MRI guidance using robotic assistance," in *Proc. IEEE Int. Conf. Robot. Autom. (ICRA)*, 2010, pp. 2574–2579.

- [19] J. Stoll and P. Dupont, "Passive markers for ultrasound tracking of surgical instruments," *Med. Image Comput. Comput.-Assist. Intervention (MICCAI)*, (Lecture Notes in Computer Science, vol. 3750), pp. 41–48, 2005.
- [20] K. A. Horvath, M. Guttman, M. Li, R. Lederman, D. Mazilu, O. Kocaturk, P. Karmarkar, T. Hunt, S. Kozlov, and E. McVeigh, "Beating heart aortic valve replacement using real-time MRI guidance," *Innovations*, vol. 2, pp. 51–55, 2007.
- [21] E. R. McVeigh, M. Guttman, R. Lederman, M. Li, O. Kocaturk, T. Hunt, S. Kozlov, and K. Horvath, "Real-time interactive MRI-guided cardiac surgery: Aortic valve replacement using a direct apical approach," *Magn Reson. Med.*, vol. 56, pp. 958–964, 2006.
- [22] M. Guttman, P. Kellman, A. Dick, R. Lederman, and E. McVeigh, "Real-time accelerated interactive MRI with adaptive TSENSE and UNFOLD," *Magn. Reson. Med.*, vol. 50, pp. 315–321, 2003.
- [23] A. Kapoor, B. Wood, D. Mazilu, K. A. Horvath, and M. Li, "MR-compatible hands-on cooperative control of a pneumatically actuated robot," in *Proc. IEEE Int. Conf. Robot. Autom. (ICRA)*, pp. 2681–2686, 2009.
- [24] K. Chinzei, R. Kikinis, and F. Jolesz, "MR compatibility of mechatronic devices: design criteria," *Med. Image Comput. Comput.-Assist. Intervention (MICCAI)*, (Lecture Notes in Computer Science, vol. 1679), pp. 1020–1031, 1999.
- [25] J. F. Schenck, "Safety of strong, static magnetic fields," *J. Magn. Reson. Imag.*, vol. 12, pp. 2–19, 2000.
- [26] A. Patriciu, D. Petrisor, M. Muntener, D. Mazilu, M. SchLr, and D. Stoianovici, "Automatic brachytherapy seed placement under MRI guidance," *IEEE Trans. Biomed. Eng.*, vol. 54, no. 8, pp. 1499–1506, Aug. 2007.
- [27] S. P. DiMaio, E. Samset, G. Fischer, I. Iordachita, G. Fichtinger, F. Jolesz, and C. M. Tempny, "Dynamic MRI scan plane control for passive tracking of instruments and devices," *Med. Image Comput. Comput.-Assist. Intervention (MICCAI)*, (Lecture Notes in Computer Science, vol. 4792), pp. 50–58, 2007.



**Ming Li** (S'03–M'06) received the B.Sc. degree in biomedical engineering from Shanghai Jiao Tong University, Shanghai, China, in 1992, the M.E. degree in precision machinery engineering from the University of Tokyo, Tokyo, Japan, in 2000, and the Ph.D. degree in computer science from the Johns Hopkins University, Baltimore, MD, in 2005.

In 2005, she joined National Institutes of Health, Bethesda, MD, as a Staff Scientist. She is currently the bioengineering section Chief of Cardiothoracic Surgery Research Program, National Heart, Lung and

Blood Institute, National Institutes of Health. Her research interests include medical robotics, surgical navigation, medical imaging, human-machine interaction, and system integration.



**Ankur Kapoor** (S'04–M'07) received the Bachelor of Engineering degree (with highest honors) in mechanical and electrical and electronics from the Birla Institute of Technology and Science, Pilani, India, in 2000, and the M.S. degree in computer science and the Ph.D. degree in computer science from the Johns Hopkins University, Baltimore, MD, in 2006 and 2007, respectively.

Since the fall of 2007, he has been a Research Fellow at Radiology and Imaging Sciences, Clinical Center, National Institutes of Health, Bethesda, MD.

His research interests include robot assisted minimally invasive surgery, architecture for surgical systems, and image or visually guided interventions and surgery.



**Dumitru Mazilu** (M'01) received the B.Sc. degree and the Ph.D. degree in mechanical engineering from University of Craiova, Romania, in 1984 and 1998, respectively.

He was a Research Fellow at the Johns Hopkins University, Baltimore, MD, in 2000. From 2003 to 2006, he was a Research Associate in the Urology Department, Johns Hopkins University, Baltimore, MD. He is currently a Research Scientist at the National Institutes of Health, Bethesda, MD. His current research interest include the design of medical robotics

and medical devices. He is the author or coauthor of numerous scientific papers and several national and international patents. During his career he participated in the design and development of several medical robots and medical devices.



**Keith A. Horvath** received the B.S. degree in biochemistry and the M.D. degree from the University of Chicago, Chicago, IL, in 1983 and 1987, respectively. He finished his training in general and cardiothoracic surgery at the Brigham and Women's Hospital.

He joined the cardiac surgical faculty at Northwestern University, Chicago, IL, in 1996. In 2004, he moved to the National Institutes of Health. He is currently the Chief of the Cardiothoracic Surgery at Suburban Hospital, as well as the Director of the Cardiothoracic Surgery Research, National Heart, Lung,

Blood Institute, National Institutes of Health, Bethesda, MD, and an affiliate with Johns Hopkins Medical Center. His research interests include minimally invasive cardiac surgery, robotic assisted cardiac surgery, stem cell therapy, and xenotransplantation.